

Lead-free MDABCO-NH₄I₃ perovskite crystals embedded in electrospun nanofibers

Rosa Baptista ^{1,*}, Gonalo Moreira ¹, Bruna Silva ¹, Joo Oliveira ¹, Bernardo Almeida ¹, Cidlia Castro ², Pedro V. Rodrigues ², Ana Machado ², Michael Belsley ² and Etelvina de Matos Gomes ²

^a Centre of Physics of Minho and Porto Universities (CF-UM-UP), University of Minho, Campus de Gualtar, 4710-057 Braga, Portugal

^b Institute for Polymers and Composites, University of Minho, Campus de Azurm, 4800-058 Guimares

*Corresponding author: rosa_baptista@fisica.uminho.pt

Supplementary Information

SI1. XRD crystallites size

Estimates of the nanocrystal size, d , was obtained using the Scherrer equation

$$\beta_{hkl} = \frac{K\lambda}{d\cos\theta} \quad (1)$$

Here K is a correction factor to particle shape and λ the X-ray wavelength. In the absence of detailed shape information, a value of $K = 0.90$ is commonly used ^[1]. The full width of the diffraction peak at half the maximum (FWHM) gives the broadening of a (hkl) reflection and is expressed as β_{hkl} . To estimate the FWHM, first the main peaks were eliminated from the spectra and a cubic spline was globally fit to the resulting background using the MATLAB application “shape language modeling” ^[2].

Subsequently each individual background corrected peak was fit to and asymmetric Pseudo-Voigt profile using the MATLAB nonlinear least squares fitting algorithm. The Pseudo-Voigt function is,

$$I = A[\eta L(x) + (1 - \eta)G(x)] \quad (2)$$

Representing a weighted linear superposition of Lorentz $L(x)$ and Gauss $G(x)$ functions. Here the parameter η represents the fractional contribution of the Lorentz function while the parameter A is proportional to the amplitude of the

diffraction peak above the background. The Lorentzian and Gaussian functions are:

$$L(x) = \frac{(2/\pi\beta^*)}{1+4x^2}$$

$$G(x) = \frac{2}{\beta^*} \sqrt{\frac{\ln(2)}{\pi}} \exp(-4\ln(2)x^2)$$
(2a)

written in terms of the scaled diffraction angle

$$x = \frac{2(2\theta - 2\theta_c)}{\beta^*}$$
(2b)

and the asymmetric width function^[3]

$$\beta^* = \frac{2\beta}{1 + \exp[a(2\theta - 2\theta_c)]}$$
(2c)

In these expressions, the calculated peak position is $2\theta_c$ and a represents the asymmetry parameter.

The resulting fits are shown in Figure S1 a) to) while Tables S1 and S2 list the fit parameter values ($A, \eta, \theta_c, \beta, a$) for the two peaks ($11\bar{1}$) and (200). The red shading in Figure S1 represents the 68% confidence intervals of the fit peaks.

Table S1: Fit parameter values for the MDABCO-NH₄I₃ embedded into PVC, PA66 and PMMA correspondent to Bragg reflection ($11\bar{1}$).

	A	η	$2\theta_c$	β	a
MDABCO-NH ₄ I ₃ @ PVC	9.02	1.00	21.947°	0.124°	-6.35
MDABCO-NH ₄ I ₃ @ PA66	12.639	1.00	21.941°	0.099°	-2.45
MDABCO-NH ₄ I ₃ @ PMMA	19.50	1.00	21.883	0.100°	4.846

Table S2: Fit parameter values for the MDABCO-NH₄I₃ embedded into PVC, PA66 and PMMA correspondent to Bragg reflection (200).

	A	η	$2\theta_c$	β	a
MDABCO-NH ₄ I ₃ @ PVC	12.84	0.60	24.676°	0.158°	16.51
MDABCO-NH ₄ I ₃ @ PA66	9.07	1.00	24.702°	0.103°	6.37
MDABCO-NH ₄ I ₃ @ PMMA	14.10	0.65	24.649°	0.121°	3.53

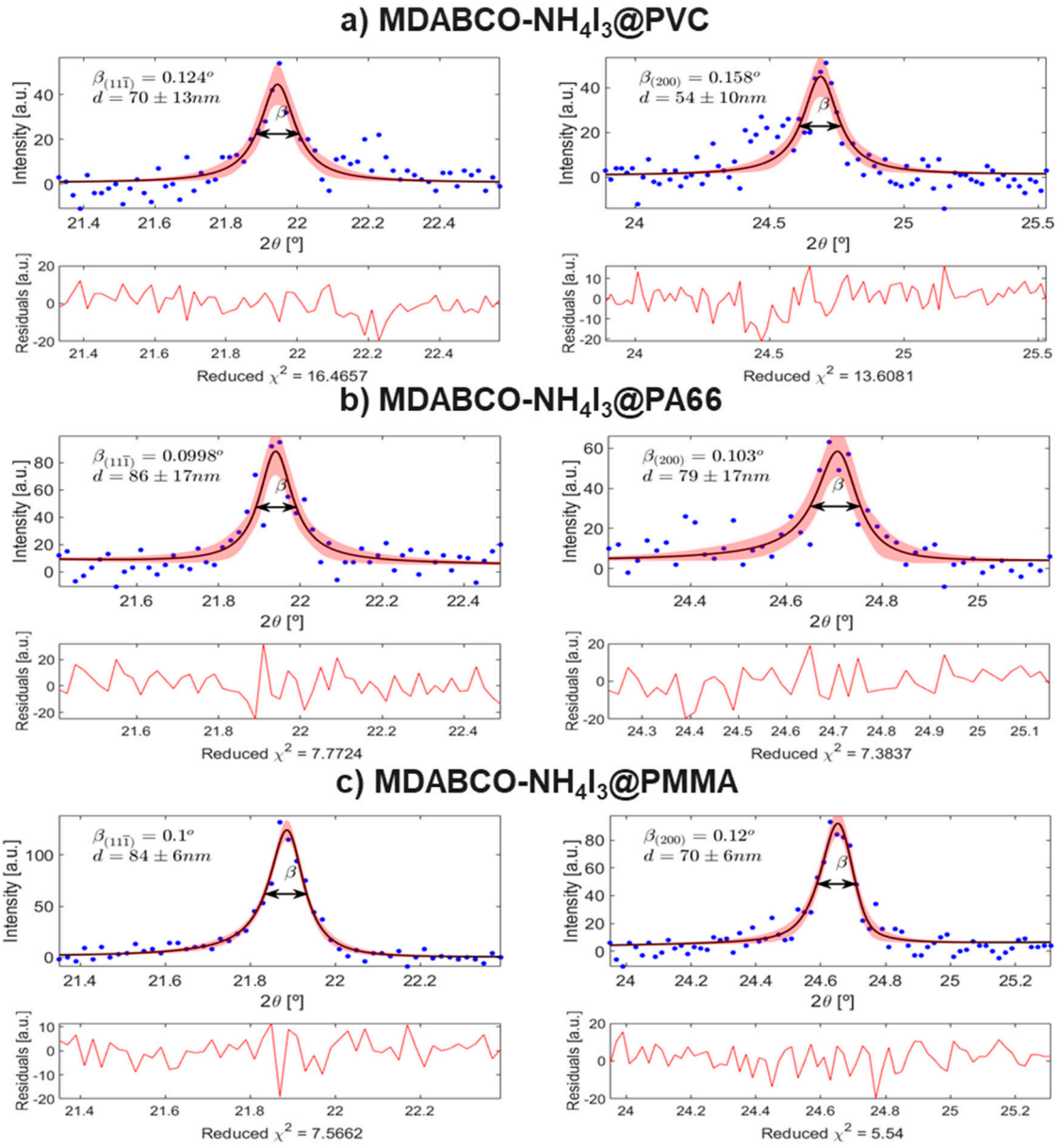


Figure S1. Asymmetric Pseudo-Voigt fits of the (111) and (200) Bragg reflections for MDABCO-NH₄I₃ crystals inside a) PVC, b) PA66 and c) PMMA nanofibers. The width of the reflections at half the maximum β and the nanocrystals average size d is indicated as well the refit residuals.

S2. UV-Visible Reflectance Spectra

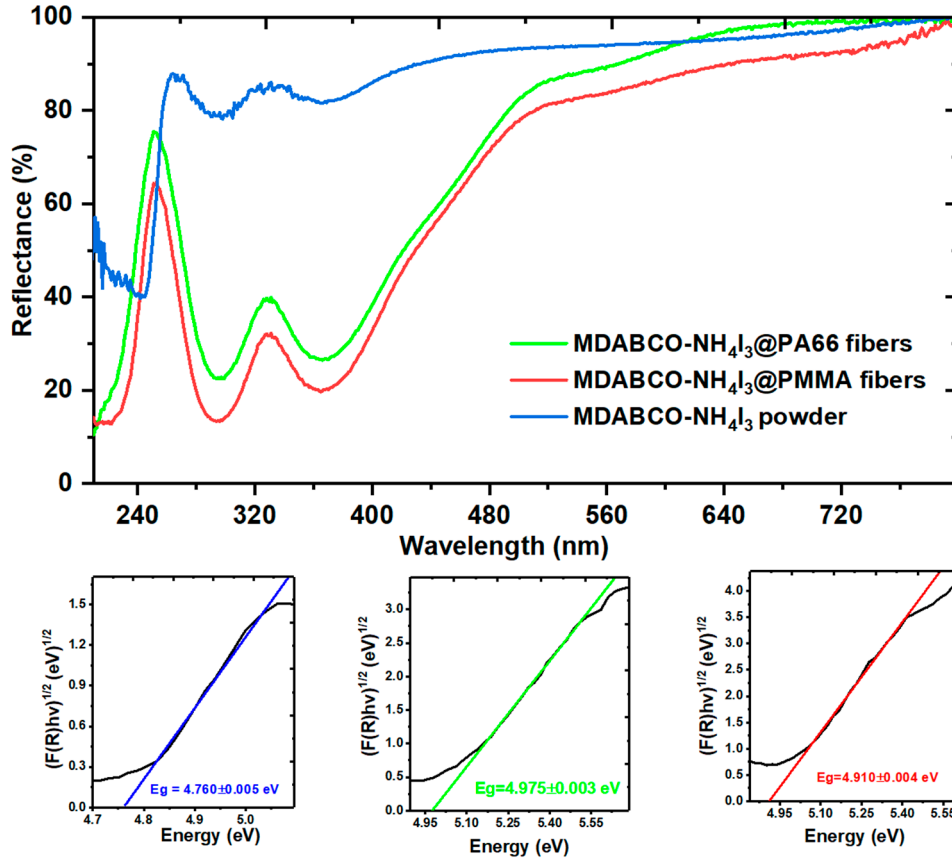


Figure S2. UV-vis reflectance of MDABCO-NH₄I₃ powder pellet and electrospun fibers. The inset shows the Kubelka-Munk function indicating a band gap energy of 4.760 eV for the polycrystalline perovskite, 4.975 eV and 4.910 eV for MDABCO-NH₄I₃@PA66 and MDABCO-NH₄I₃@PMMA nanofibers, respectively.

S3. DSC analysis

In figure S3, the measured DSC of synthesized MDABCO-NH₄I₃ perovskite crystals, showed the ferroelectric-paraelectric phase transition to occur at 443 K with area 19.9 J/g. MDABCO-NH₄I₃ perovskite crystals start to decompose above 460 K with the formation of NH₄IO₃. Cooling down from 473 K, shows a peak at 350 K, area -13.26 J/g. During the second heating, a peak with maximum at 358 K and area 12.3 J/g is observed. These two peaks correspond respectively to the paraelectric to ferroelectric and ferroelectric-paraelectric phase transitions of

NH_4IO_3 compound, which was formed after the first heating ^[4]. The perovskite phase transition at 443 K is not recovered, which reveals that crystal thermal degradation starts above 460 K^[5].

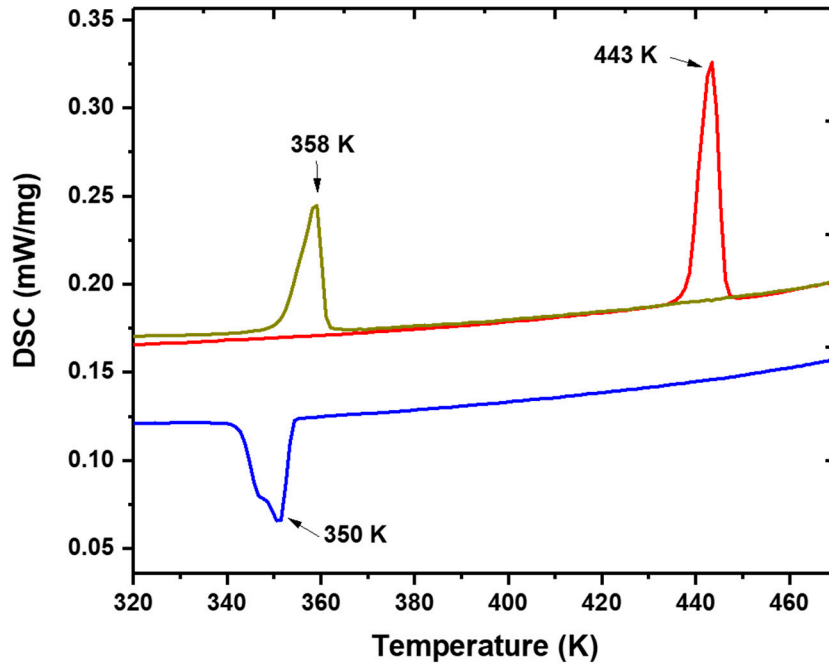


Figure S3. DSC spectra of synthesized MDABCO-NH₄I₃ perovskite crystals.

S4. RAMAN Spectra

In Figure S4, the measured Raman modes between 50 – 600 cm^{-1} are shown for a MDABCO-NH₄I₃ polycrystalline sample, for electrospun fibers of PVC and MDABCO-NH₄I₃@PVC. In the spectra, the low frequency modes are due to lattice vibrations. From the two bands at 68 cm^{-1} and 103 cm^{-1} present in the polycrystalline sample, only the second band (now shifted to 109 cm^{-1}) remains intense for the perovskite nanocrystals embedded in the polymer fibers. The strong decreasing in intensity of the 68 cm^{-1} band is probably the result of constraints imposed by the polymer matrix on the lattice vibrations modes, due to crystal confinement.

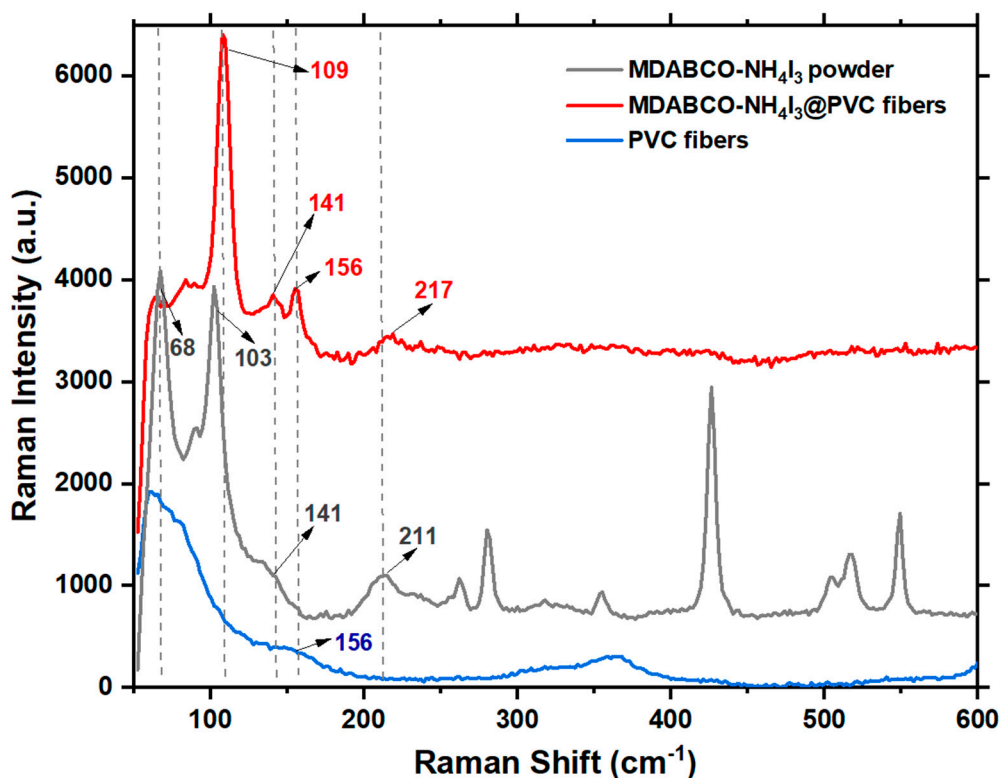


Figure S4. Raman spectra for MDABCO-NH₄I₃ polycrystalline sample (black line), for electrospun fibers of PVC (blue line) and MDABCO-NH₄I₃@PVC fibers (red line), expansion between 50 – 600 cm^{-1} .

The weak broad bands centred at 141 cm^{-1} for polycrystalline MDABCO-NH₄I₃ and 156 cm^{-1} for PVC fibers, are resolved into well-defined bands for MDABCO-NH₄I₃@PVC fibers. The weak band for MDABCO-NH₄I₃ at 211 cm^{-1} is slightly shifted to 217 cm^{-1} , for the perovskite incorporated into the fibers.

Noticed that for MDABCO-NH₄I₃@PVC fibers, none of the Raman peaks between 250 – 600 cm^{-1} are perceptible, while they are present in the MDABCO-NH₄I₃ perovskite spectra. We may conclude that the polymer matrix strongly constrains these perovskite vibrational modes as mentioned above, which is expectable as the fibers were electrospun from a precursor solution with ration of MDABCO-NH₄I₃ to PVC of 1:5.

S5. FTIR-ATR analysis

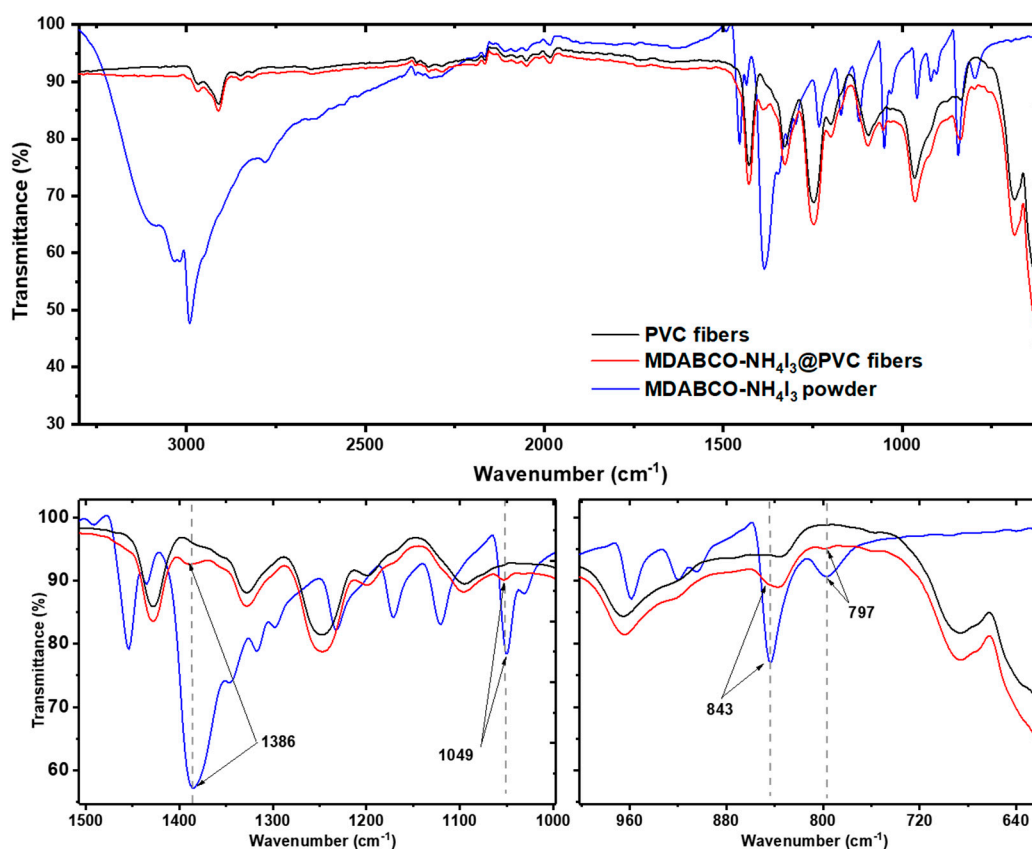


Figure S5. FTIR-ATR spectra of PVC polymer, MDABCO-NH₄I₃ powder and MDABCO-NH₄I₃@PVC fibers, a) full measurement and b) expansion between 1000 – 1500 cm^{-1} and 600 – 1000 cm^{-1} .

In Figure S5 b), the measured FTIR-ATR between 1500 – 600 cm^{-1} is shown for a MDABCO-NH₄I₃ polycrystalline sample, for electrospun fibers of PVC and MDABCO-NH₄I₃@PVC. Slight differences were observed between the spectra of electrospun fibers of PVC and MDABCO-NH₄I₃@PVC, and just few bands (the most intense) were possible to be assigned to MDABCO-NH₄I₃ perovskite nanocrystals at the 1386 cm^{-1} , 1049 cm^{-1} , 843 cm^{-1} and 797 cm^{-1} . However, the strong decreasing in intensity observed for the perovskite bands on electrospun fibers of MDABCO-NH₄I₃@PVC sample is due to the sobreposition of the polymer bands to those of MDABCO-NH₄I₃ crystals. As already mentioned, the ratio perovskite and polymer are 1:5, on the precursor solution used to fabricate

the electrospun fibers. Therefore, is expected that the only the stronger perovskite bands will be observed. That contained a concentration constrain imposed by the polymer matrix on the IR bands.

S6. Piezoelectric nanogenerator

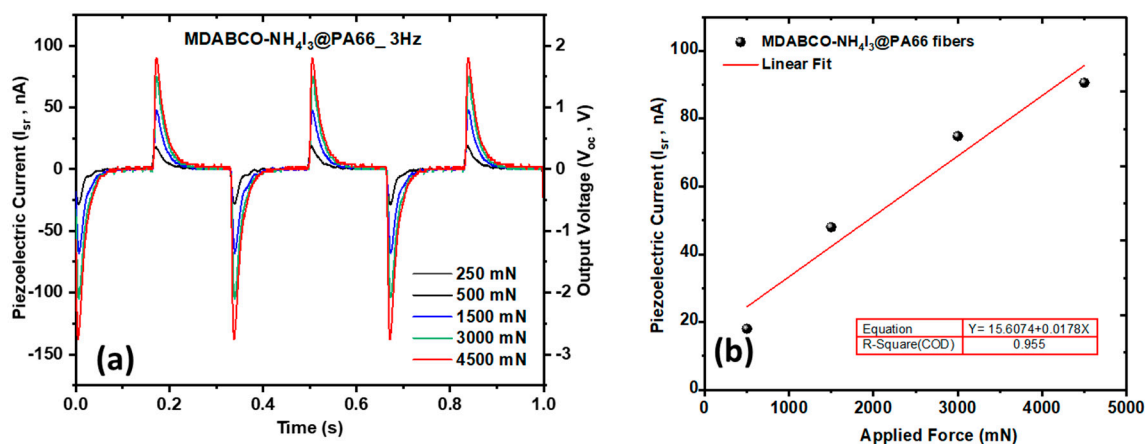


Figure S6. MDABCO-NH₄I₃@PA66 fibers (a) Piezoelectric current as function of time, for several applied forces and (b) linear fitting.

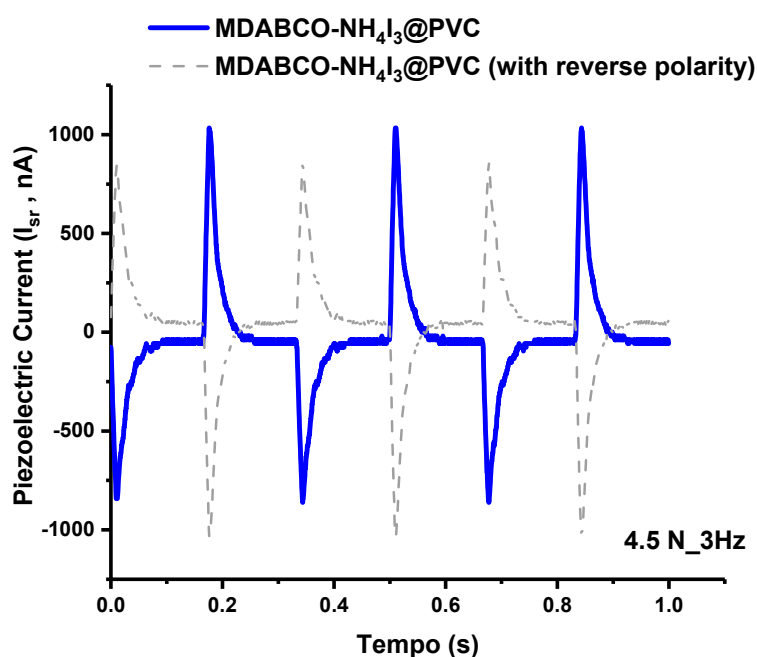


Figure S7. Output voltage generated from MDABCO-NH₄I₃@PVC nanofiber mat with reverse polarity.

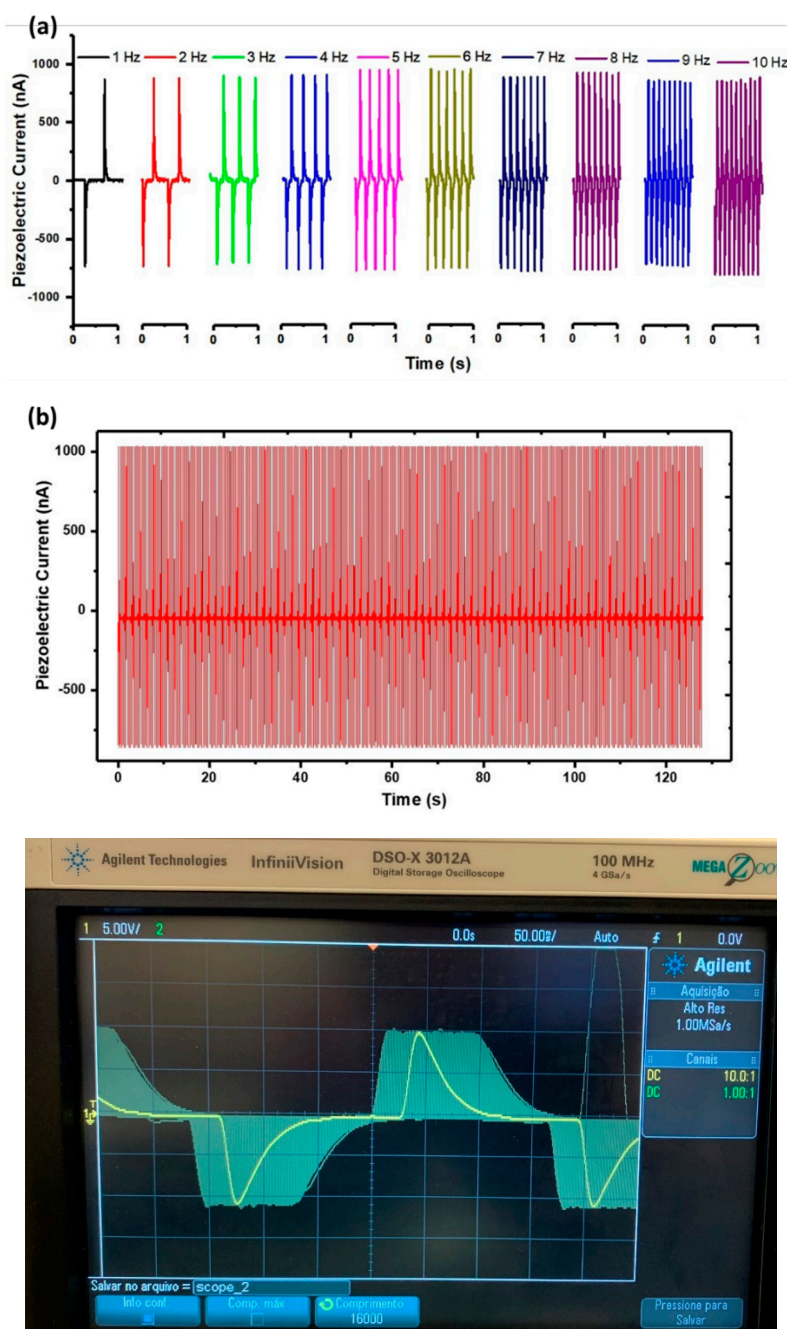


Figure S8. MDABCO-NH₄I₃@PVC nanofiber mat piezoelectric current generated a) for frequencies between 1Hz and 10 Hz and b) a 130 s interval under a periodical force applied with 4.5 N. A stability test was performed during a time interval of 4 h under a periodical force applied with 2.7 N at a frequency of 3 Hz (oscilloscope image).

S9. Mechanical Properties

Tensile strain applied to PVC and MDABCO-NH₄I₃@PVC electrospun fiber mat are shown in Figure S9. The results from tensile measurements show that MDABCO-NH₄I₃@PVC fibers exhibit good mechanical performance with an average increase of 14% on tensile strength (reaching ~ 4.0 MPa) and an increase of 40% on the strength at yield reaching (~ 2.5 MPa) when compared with PVC fibers. More importantly, the Young modulus increases from ~20 MPa in PVC fibers to ~58 MPa in MDABCO-NH₄I₃@PVC fibers, an increase of around 66%. This significant increase of the Young modulus of perovskite doped electrospun fibers indicates that composite MDABCO-NH₄I₃@PVC are mechanically stronger than neat polymer fibers. This is very important for the performance of MDABCO-NH₄I₃@PVC fiber mat as nanogenerator as it will increase its capability of supporting longer times under applied external force.

The decrease of 30% on the strain at break for doped fibers indicates a decrease in their plasticity, which might result from the presence of nanocrystals inside the PVC polymer which inhibits the capability for the PVC chains to flow between.^[6]

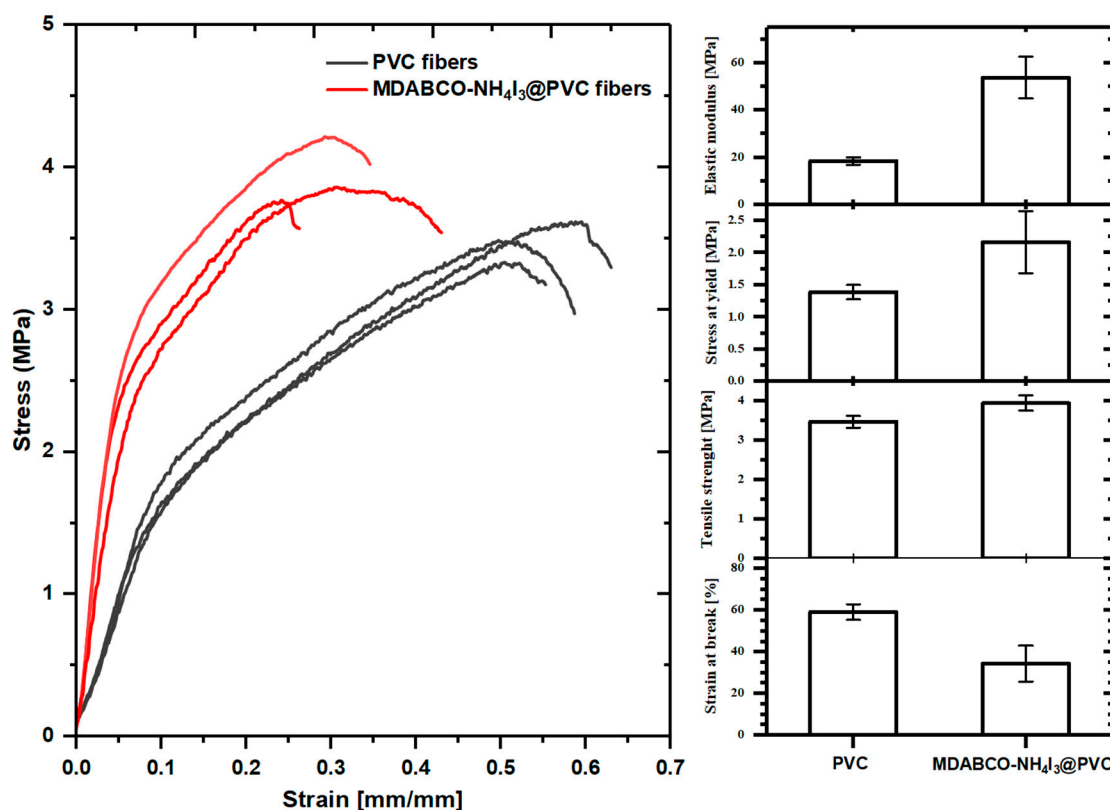


Figure S9. Elastic modulus, stress at yield, tensile strength and strain at break of PVC and MDABCO-NH₄I₃@PVC electrospun fibers.

References

- (1) Klug, H.; Alexander, L., *X-Ray Diffraction Procedures 2nd edn*, Ch. 9. Wiley: 1974.
- (2) John D'Errico (2022). SLM - Shape Language Modeling.
<https://www.mathworks.com/matlabcentral/fileexchange/24443-slm-shape-language-modeling>), MATLAB Central File Exchange. Retrieved July 5, 2022.
- (3) Stancik, A. L.; Brauns, E. B. A simple asymmetric lineshape for fitting infrared absorption spectra. *Vib Spectrosc* **2008**, 47 (1), 66-69, DOI: <https://doi.org/10.1016/j.vibspec.2008.02.009>.
- (4) Keve, E. T.; Abrahams, S. C.; Bernstein, J. L. Pyroelectric Ammonium Iodate, a Potential Ferroelastic: Crystal Structure. *The Journal of Chemical Physics* **1971**, 54 (6), 2556-2563, <https://doi.org/10.1063/1.1675212>.

- (5) Sirbu, D.; Tsui, H. C. L.; Alsaif, N.; Iglesias-Porras, S.; Zhang, Y.; Wang, M.; Liu, M.; Peacock, A. C.; Docampo, P.; Healy, N. Wide-Band-Gap Metal-Free Perovskite for Third-Order Nonlinear Optics. *Acs Photonics* **2021**, 8 (8), 2450-2458, <https://doi.org/10.1021/acsp Photonics.1c00687>.
- (6) Lee, D. W.; De Los Santos V, L.; Seo, J. W.; Felix, L. L.; Bustamante D, A.; Cole, J. M.; Barnes, C. H. W. The Structure of Graphite Oxide: Investigation of Its Surface Chemical Groups. *The Journal of Physical Chemistry B* **2010**, 114 (17), 5723-5728, <https://doi.org/10.1021/jp1002275>.